Isolation Enhancement of Tightly Coupled Dual-band MIMO DRA Antennas Using Dual-band Metasurface for Low Cost 5G Applications

Muhammad Yasir Jamal[1, 2], Min Li[1], Hashibul Alam[3], and Lijun Jiang[1]
1University of Hong Kong, Department of Electrical and Electronic Engineering, Hong Kong
2University of Engineering and Technology, Lahore, Pakistan
3Aliah University, Kolkata India
*Correspondence: engryasir1986@gmail.com , minli@eee.hku.hk, jianglj@hku.hk,

Citation | Jamal. M. Y, Li. M, Alam. H, Jiang. L, "Isolation Enhancement of Tightly Coupled Dual-band MIMO DRA Antennas Using Dual-band Metasurface for Low Cost 5G Applications", IJIST, Vol. 8 Issue. 2 pp 685-697, April 2026
Received | March 14, 2026 **Revised |** April 16, 2026 **Accepted |** April 21, 2026 **Published |** April 26, 2026.

In this research work, a dual-band metasurface has been proposed in order to increase the isolation between two closely packed dual-band dielectric resonator antennas (DRAs). The metasurface has been placed only 0.08λo away from the antennas at the center frequency of the lower band. The proposed dual-band metasurface unit cell consists of two copper traces of different lengths printed on both sides of a printed circuit board (PCB). High isolation of more than 20 dB has been achieved for 3.4 and 4.9 GHz 5G bands with impedance bandwidths of more than 200 MHz and 1.4 GHz respectively. The antenna exhibits excellent compactness by reducing the spacing between radiating elements to 0.12λo at 3.5 GHz. The proposed isolation technique can be useful for the applications where PCB of the antenna system is not allowed to be modified.

Keywords: Isolation, DRA Array, Dual-Band, Metasurface, Metamaterial Decoupling, MIMO Antenna, PCB, Sub-6 GHz 5G, Mutual Coupling Reduction

Introduction:

The rapid advancement in wireless communication and the emergence of 5G technology have necessitated antenna designs that support multi-band operation to optimize space utilization. Multiple-input multiple-output (MIMO) technology has become an increasingly important area of research due to its suitability for 5G communications. MIMO antenna systems enhance channel capacity and spectral efficiency by employing multiple antennas at both the transmitting and receiving ends, thereby improving power efficiency and bandwidth [1].

Despite these advantages, a key practical challenge in implementing MIMO systems is the close placement of antenna elements. Such proximity results in strong mutual coupling due to radiation interactions, which degrades system performance. Therefore, MIMO antenna systems must achieve high isolation with minimal coupling between elements [2].

Consequently, there is a critical need to develop effective isolation techniques for multiband antennas to mitigate the effects of close spacing and coupling. In this context, [3] proposed a mutual coupling suppression technique based on a metamaterial superstrate placed between the elements of a densely packed micro strip phased array. Extensive work has been carried out in the past on isolation techniques for dual-band operation [4][5][6][7][8][9][10][11][12][13][14][15][16][17][18][19][20][21][22][23]. In these works, the isolation was provided through the methods of defected ground slot (DGS), neutralization lines, parasitic elements, and orthogonal polarizations. However, the major drawback of these isolation techniques is that they provide isolation either through the modification of the antenna PCB or through the antenna dependency. Keeping in view the issues associated with these isolation methods, recent works [24] have presented the idea of metasurfaces because of their attractive properties. The metasurfaces, for instance, electromagnetic band gap (EBG), spoof surface Plasmon Polariton (SSPP), and waveguide metamaterials [24][25][15] have been applied efficiently to achieve effective dual-band decoupling. However, it has been observed that these metamaterial designs present relatively high complexity and usually require larger spacing between antenna and metasurface. Therefore, such metamaterial designs are not suitable candidates for certain situations and are less suitable for compact antenna designs. A compact size of dual-band low-loss aperture-coupled dielectric resonator antenna for C and X Band Applications has been addressed in [26].

Nowadays, DRAs are becoming increasingly popular in MIMO technology due to their alluring features such as compact size, high efficiency, and versatile excitation techniques [27]. Various isolation enhancement techniques have been explored as well for MIMO DRA [28][29][30][31][32][33][34]. Unfortunately, most of them are only for single-band operation, not for multi-band operation. Later, several works presented multi-band isolation techniques in MIMO DRA [35][36] by (i) large spacing between antennas, (ii) special shape of the antenna, and (iii) modifying PCB. Some recently reported works [37][38][39] lack simplicity, require PCB modification, or do not support the sub-6 GHz band. Even so, most proposed isolation methods for multi-band MIMO DRAs cannot be implemented where modification of the PCB or antenna shape is not permitted. Most existing isolation techniques either modify the antenna PCB, rely on large spacing between elements, or are limited to single-band operation. The proposed metasurface approach addresses these limitations by enabling compact dual-band isolation without modifying the antenna PCB. Thus, it may be concluded that there is a strong need to explore a simple and compact multi-band MIMO DRA decoupling technique, which may be used without any modification for antenna system PCB.

This work presents a novel isolation enhancement technique in MIMO DRA for a dual-band decoupling design by using a metasurface. By introducing a very simple and compact metasurface (two copper traces of different lengths printed on both sides of a printed circuit board), as a superstrate, the dual-band DRA antenna is successfully decoupled for sub-6 GHz

5G bands. The obtained results showed that the proposed antenna system has been able to achieve more than 20 dB of isolation for 3.3-3.5 and 4.8-5 GHz frequency bands.

Design Configuration:

Figure 1 presents the schematic diagram of the proposed MIMO DRA, where the antenna is composed of a metasurface and two closely packed DRA. The proposed design of antenna has been developed in two sections as described below. At first, a single dual-band DRA has been developed, followed by the design of the proposed metasurface. For developing DRA in this work, the dielectric material has ε_r =10, because such material value helps achieve the maximum bandwidth [40]. It is worth mentioning that the smaller ε_r values of dielectric material show the problem of coupling; whereas, larger ε_r values suffer from a high Q-factor. Both of these factors can hinder the achievement of high DRA bandwidth. The antenna is simulated in CST. The simulation employs open boundary conditions with the frequency-domain solver and adaptive mesh refinement to ensure accurate S-parameter results.

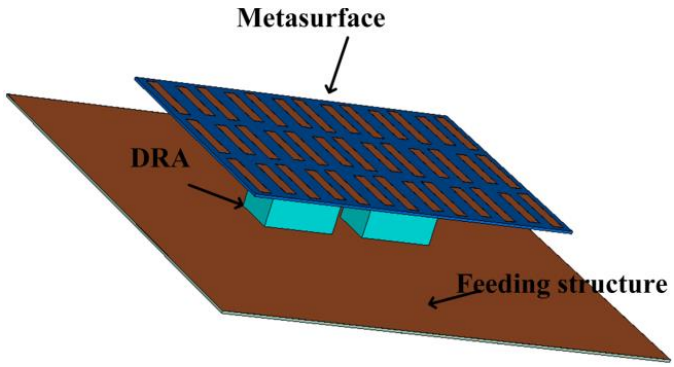

Figure 1. Proposed antenna configuration.

Figure 2 shows the model of a single dual-band DRA. The base model of DRA has been designed by equations from [26] and DRA dimensions are calculated according to these equations. For DRA shown in Fig. 2(a), when W_d, H_d < L_d, TE_{111} is the dominant mode and the higher-order mode TE_{112} is excited for dual-band frequency response. When a dielectric resonator antenna (DRA) is excited, it supports discrete electromagnetic field patterns called modes. The notation TEmnp describes how the fields vary inside the dielectric along three orthogonal directions (length, width and height). Eqns. (1) and (2) can be used to estimate the dimension W_d, H_d of the antenna with m=1 and n=1. Furthermore, for a well-guided mode i.e. due to high permittivity material, Eqns. (1) and (2) can be approximated as Eqns. (3) and (4). Where k_x and k_y are the wavenumbers in the x and y directions, and k_0 is the free space wavenumber given by (5). Using Eqns. (3) and (4), W_d, H_d can be chosen as the guided half wavelength at the desired frequencies [26]. In the proposed design, the desired frequencies of 3.4 and 4.5 GHz correspond to W_d =13.92 mm and H_d =11 mm respectively. Due to fringing fields between the DRA and air interface, certain optimizations are needed. A microstrip line has been used to feed the DRA through a slot as shown in Figure 2(b). The length of the slot can be estimated using Eqn (6) and λ_0 is the wavelength at 3.4 GHz. The ε_r and ε_{r1} are the dielectric constants of DRA material and feeding substrate, respectively. The feeding substrate in the proposed design is Rogers RO4350B with ε_{r1}=3.66. Using Eqn. (6), the slot length is found to be as L_s =13.3 mm while the width of the slot is chosen as W_s =0.2×L_s=2.66 mm. The width of the feeding micro strip line is W_f =1.8 mm which corresponds to 50 Ω impedance. The length of the micro strip line is optimized as L_f=77.9 mm for good impedance matching. After using CST optimizations, the final DRA and feeding dimensions are W_d=14.6 mm, H_d=15 mm, L_d=22.54 mm, W_f=1.8 mm, L_f=77.9 mm, L_s=12.4 mm and W_s=2.1 mm.

Equations(1)-(5) are used to design DRA antenna dimensions [26] and equation (6) for the dimension of feeding slot.

$$k_x = \frac{m\pi}{W_d}\left(1+\frac{2}{W_d k_0(\sqrt{\varepsilon_r}-1)}\right) \quad (1)$$

$$k_y = \frac{n\pi}{H_d}\left(1+\frac{2}{H_d k_0(\sqrt{\varepsilon_r}-1)}\right) \quad (2)$$

$$k_x = \frac{m\pi}{W_d} \quad (3)$$

$$k_y = \frac{n\pi}{H_d} \quad (4)$$

$$k_0 = \frac{2\pi f_0}{c} \quad (5)$$

$$L_s = \frac{0.4\lambda_0}{\sqrt{\frac{\varepsilon_r+\varepsilon_{r1}}{2}}} \quad (6)$$

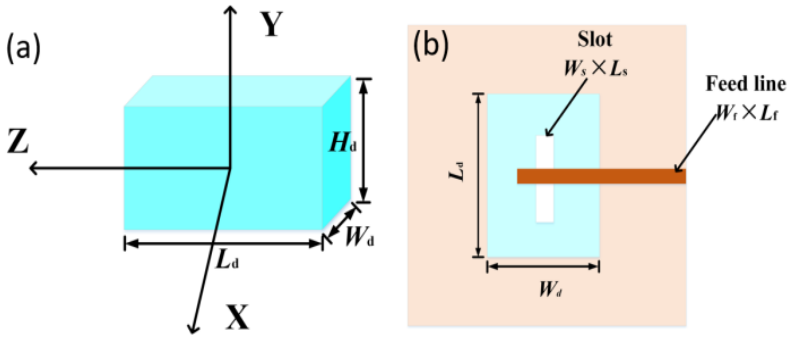

Figure 2. Dual-band DRA [26] (a) perspective view (b) top view.

Table 1. Dimensions parameter list of the antenna

Parameter	Description	Value (mm)
Wd	Width of DRA	14.6
Hd	Height of DRA	15
Ld	Length of DRA	22.54
Wf	Microstrip feed width	1.8
Lf	Microstrip feed length	77.9
Ls	Slot length	12.4
Ws	Slot width	2.1
D	Distance between DRAs	10.6
Hmeta	Height of metasurface from antennas	6.87
ld1	Length of first metasurface trace	23.4
ld2	Length of second metasurface trace	20.4
t	Trace width	3.66
G	Unit cell spacing	5.39
lgap	Gap between traces	2.15
Wm	Unit cell width	16.4

This work has presented the model composed of two dual-band DRA instead of one, as shown in Figure 3. The coupled dual-band DRA antennas are placed close to each other

with the separation distance D=10.6 mm (0.12λo at 3.5 GHz) as shown in Fig. 3(a). Figure 3(a) provides the top view of two dual-band DRA; whereas, Figure 3 (b) shows the bottom view of coupled DRA. In the figure, the materials are distinguished with different color codes. The dimensions of the ground plane are L_g=W_g=150mm. Table 1 summarizes the dimension parameters of the final antenna.

It has been noted that the antennas in DRA are strongly coupled in both the bands as can be seen from the S-parameters shown in Figure 4.

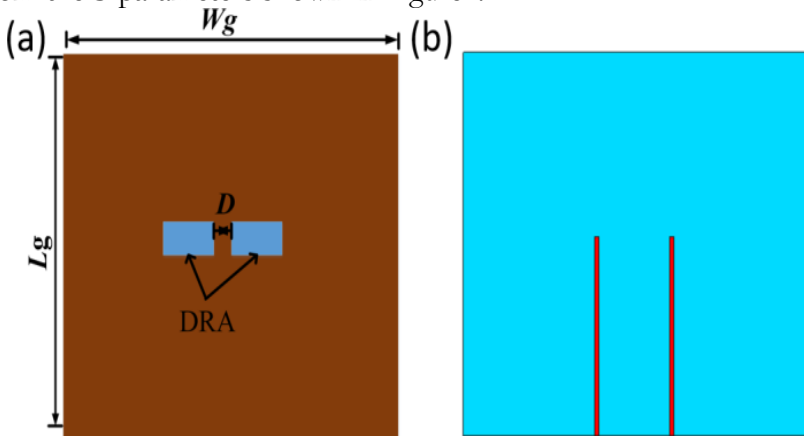

Figure 3. Coupled DRA (a) top view (b) bottom view (Rogers RO4350B: Copper:).

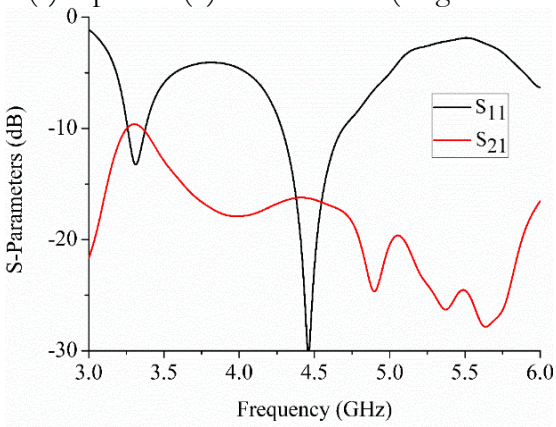

Figure 4. S-parameters of the coupled MIMO DRA antenna.

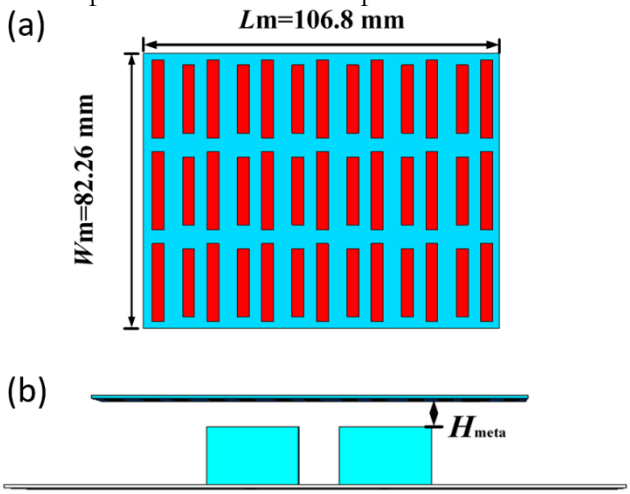

Figure 5. (a) The proposed metasurface in order to provide isolation. (b) The side views of DRAs with metasurface.

After the successful design of MIMO DRA, the next step in this work is to add the metasurface to provide isolation as shown in Figure 5. Figure 5(a) presents the proposed

design of the metasurface in this work while Fig. 5(b) shows the incorporation of the metasurface with DRA. The metasurface should be placed as close as possible to the DRA antennas to reduce the profile height. To avoid unwanted interaction between the metasurface and the fringing field of DRAs, the metasurface has been placed at a distance of H_{meta}= 6.87 mm (0.08λ_0 at 3.4 GHz) from the array as evident from the figure.

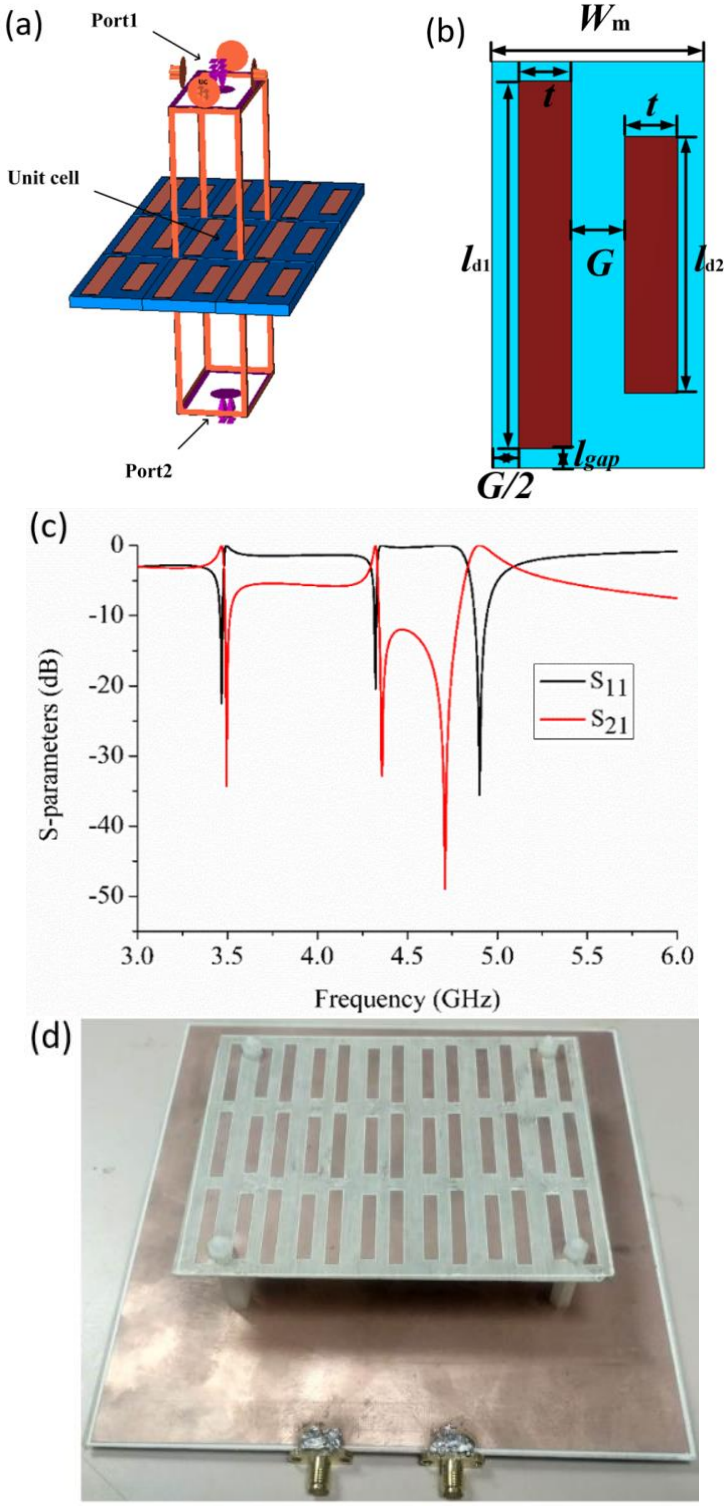

Figure 6. (a) Simulation model of the unit cell (b) dimensions of unit cell (c) S-parameters of the unit cell. (d) Fabricated antenna prototype.

The proposed metasurface consists of a periodic arrangement of the unit cell shown in Figure 6(a). The dimensions of the unit cell are shown in Figure 6(b). The unit cell consists of two metal traces of different lengths printed on both sides of a 0.8 mm thick F4B substrate. The two copper traces of different lengths act as resonant elements at two different frequencies, enabling dual-band suppression of surface waves responsible for mutual coupling. Initially, the lengths of the two traces were designed to be ld_1=27 mm, ld_2=21.8 mm. The lengths of the metallic traces were estimated based on half-wavelength resonance at the target frequencies. Subsequently, parametric optimization was carried out in CST Microwave Studio to fine-tune the trace lengths and spacing in order to achieve the desired dual-band response and maximum isolation. The S-parameters of the unit cell are plotted in Fig. 6(c), where the results show that the metasurface has a similar response as [37] at 3.5 and 4.5 GHz frequency bands. Due to the proximity effect, certain numerical optimizations are needed to achieve the best performance. The final dimensions of the metasurface unit cell are ld_1=23.4, ld_2=20.4, t=3.66, G=5.39, l_{gap}=2.15, W_m=16.4, where all units are in mm. The simulation model of the proposed metasurface with MIMO DRA has been fabricated as well and is presented in Fig. 6(d).

The S-parameter response of the unit cell is shown in Fig. 6(c). This behavior suppresses the surface waves propagating along the plane of the metasurface and consequently, helps to suppress the coupling between two antennas. A metasurface with a similar response lying in the near field was used to decouple two patch antennas.

Results and Discussion:

Figure 7(a) shows the S-parameter graph after decoupling of the antenna system. It is evident from the figure that the antenna is well-matched with S11<-10 dB and highly isolated with S21<-20 dB for 3.3-3.5 and 4.8-5 GHz frequency bands which have been designated as the sub-6 GHz bands for 5G communications. Fig. 7(b) shows the comparative results of the S-parameters for both the simulated model and fabricated prototype of the proposed design. The obtained results from the fabricated prototype verify the results obtained in the simulation. The shift may arise due to fabrication tolerances, slight variations in dielectric constant of the substrate, soldering and SMA connector losses, and assembly inaccuracies during metasurface placement. It is worth mentioning here that although the obtained results have been slightly shifted toward higher frequencies they can cover the whole of the bandwidth as apparent from Figure 7(b). It has been observed as well that the inclusion of metasurface has assisted in improving the isolation of more than 12 dB for the 3.4 GHz band and on the other hand more than 10 dB for the 4.9 GHz band.

The radiation pattern of the proposed antenna system at 3.4 and 5 GHz is shown in Figure 8. From Figure 8(a) and (b), it can be seen that the antenna has up to 30dB cross-pol discrimination in the broadside direction, which indicates very good polarization purity. The radiation pattern of the antenna is kept similar to that of the conventional DRA antenna. Figure 8(c) and (d) show the simulated radiation pattern of the antenna at 5 GHz. It can be observed that the antenna also has very good cross-pol discrimination up to 30 dB in the broadside direction at 5 GHz.

The simulated and measured radiation patterns are shown in Fig. 8(c) for both 3.4 and 5 GHz frequencies. The measured X-pol is lower than the simulated X-pol and in broadside is less than -30 dB for 3.4 GHz. For 5 GHz the measured back lobe is slightly higher but front to back ratio is higher than 10 dB. The antenna gain patterns are presented in Figure 8, illustrating the gain distribution in all directions. The radiation efficiency is more than 90 %.

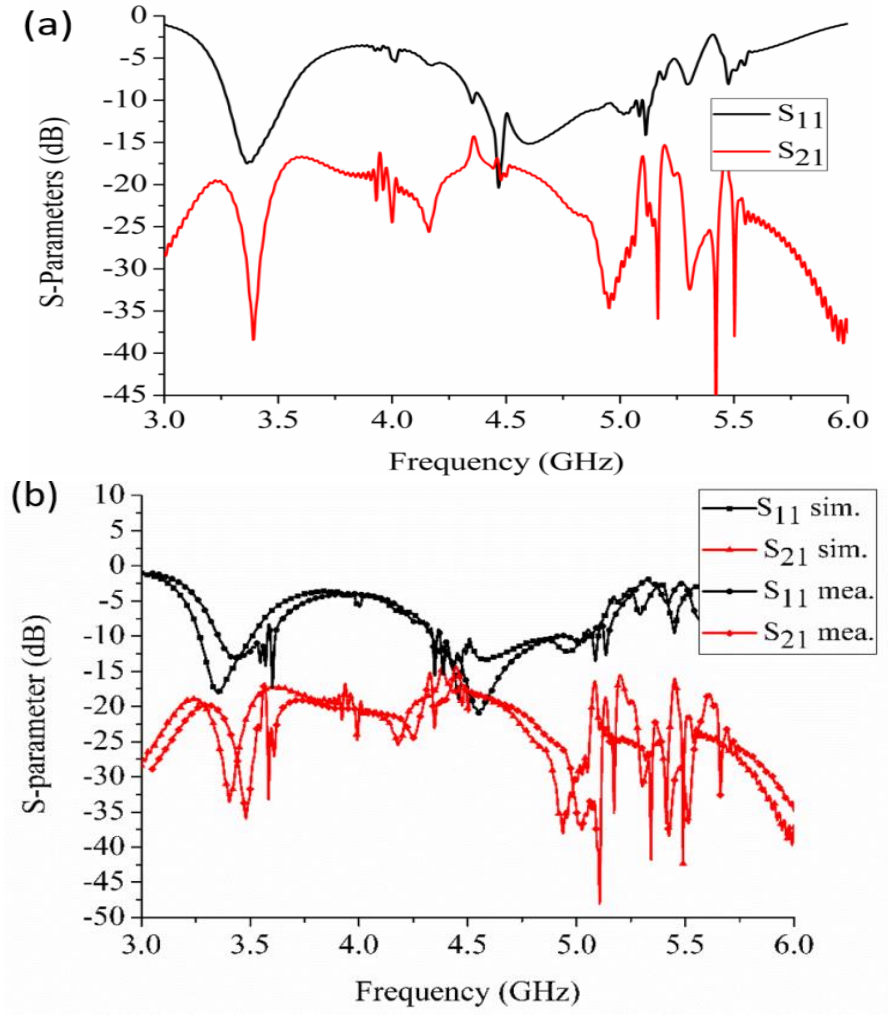

Figure 7. (a) Simulated S-parameters of the decoupled antenna. (b) Simulated and measured S-parameters of the proposed antenna.

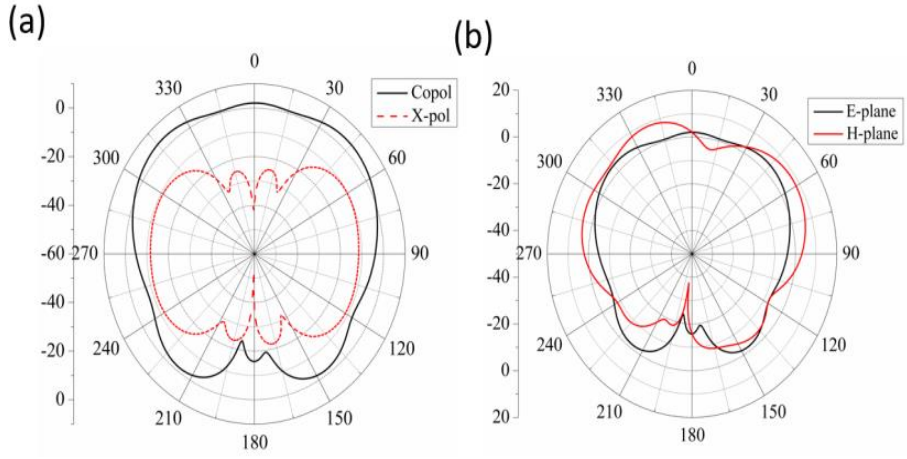

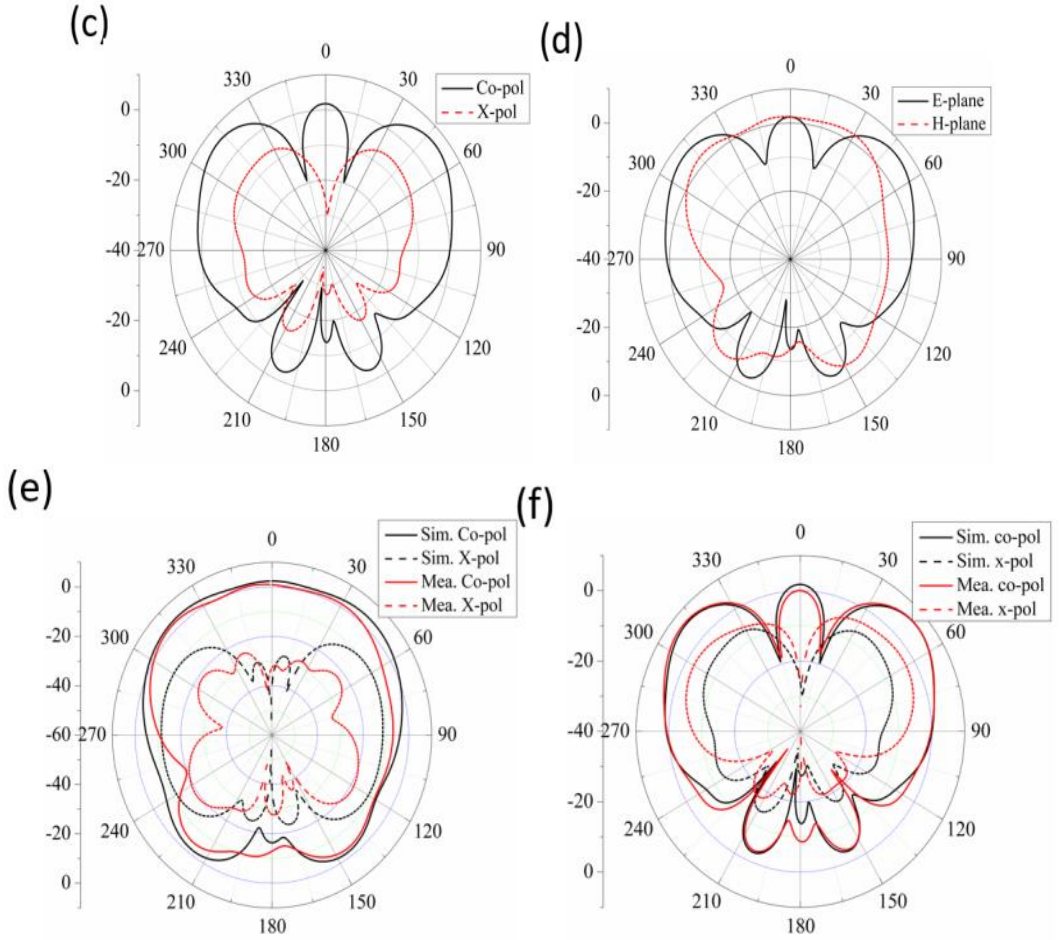

Figure 8. (a) Y-Z plane radiation pattern (b) E and H plane radiation patterns of the antenna at 3.4 GHz. (c) Y-Z plane radiation pattern (d) E and H plane radiation patterns of the antenna at 5 GHz. (e and f) Simulated and measured radiation pattern of the proposed antenna at 3.4 and 5 GHz.

Figure 9 shows the electric field distribution with and without metasurface at 3.4 GHz. From Figure 9(a) it can be observed that without using the metasurface superstrate, the antennas are strongly coupled through radiation and a large current is produced on port 2 when port 1 is excited. After adopting the isolation metasurface, the radiation interaction is reduced to a significant level, as shown in Figure 9(b). The field distribution shows that after placing the metasurface the field interaction between two antennas has been reduced significantly thereby reducing coupling which is also apparent from S12. The reason is the suppression of surface waves passing through the metasurface which minimizes the radiation coupling between the antennas. Further MIMO performance can be evaluated using ECC, DG, and TARC which are discussed below.

ECC: For a 2-port antenna, ECC (using S-parameters) can be calculated by (7):

$$\rho_e = \frac{|S_{11}S_{12}^* + S_{21}S_{22}^*|^2}{(1-|S_{11}|^2-|S_{21}|^2)(1-|S_{22}|^2-|S_{12}|^2)} \quad (7)$$

Since $S_{21}$is mostly below −15 dB → low coupling So ECC is :
< 0.05 (good) across most frequencies
Peaks near resonances (around 5–5.5 GHz)

Diversity Gain (DG):

DG is directly related to ECC by (8):

$$DG = 10\sqrt{1-\rho_e^2} \quad (8)$$

If ECC ≈ 0 → DG ≈ 10 dB (ideal)
In this case: DG ≈ 9.8–10 dB across band

Total Active Reflection Coefficient (TARC):

For a 2-port system TARC can be calculated by (9):

$$TARC = \sqrt{\frac{|S_{11}+S_{12}|^2+|S_{21}+S_{22}|^2}{2}} \quad (9)$$

TARC follows combined mismatch + coupling
Dips where antenna is well matched (same regions as S11 dips)
minima near: ~3.4 GHz ,~4.5 GHz ,~5.2–5.5 GHz.

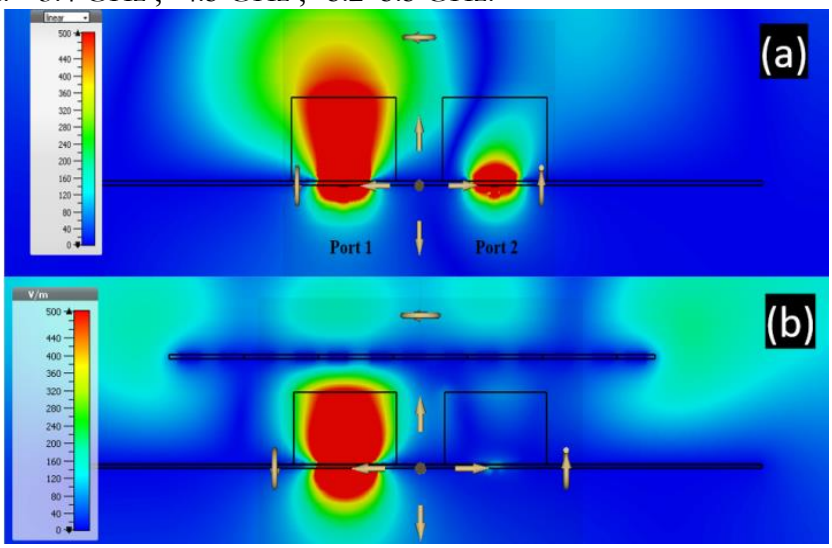

Figure 9. Electric field distribution at 3.4 GHz (a) without decoupling (b) with decoupling.

Finally, Table 2 compares the proposed antenna with previously reported antennas. The proposed design uses a novel metasurface-based decoupling technique compared to other antennas that require PCB modification. Moreover, the antenna is suitable for sub-6 GHz 5G applications.

Table 2. Comparison with Previously Reported Antennas

Ref.	Number of bands	Isolation technique	Isolation (dB)	Application
29	Single	Decoupled modes	<-20	X-band communication
33	Single	EBG	<-20	5G single band (sub-6 GHz)
36	Dual	Different excitation Techniques	-23, -32	LTE
37	Dual	Decoupled modes	-13, -16	WiMAX/WLAN
Pro.	Dual	Dual-band metasurface	<-20	5G dual-band (sub-6 GHz)

Conclusion:

In conclusion, a dual-band metasurface superstrate has been successfully proposed to enhance the isolation between two dielectric resonator antennas (DRAs) in a MIMO antenna system. Unlike most existing studies that focus on single-band DRA configurations, this work demonstrates a metasurface-based isolation technique for a dual-band system, addressing a notable gap in the literature. The proposed design achieves an isolation level exceeding 20 dB at 3.4 GHz and 4.9 GHz, which are key sub-6 GHz bands for 5G communication. Moreover, the metasurface is positioned at a compact height of only $0.08\lambda_0$ above the antennas, resulting in minimal impact on the overall profile. These characteristics make the proposed antenna system a promising solution for modern compact and low-profile wireless applications.

Acknowledgment:

The authors would like to thank the University of Hong Kong, Aliah University, and University of Engineering and Technology for their help.

References:

[1] M. A. Jensen and J. W. Wallace, "A review of antennas and propagation for MIMO wireless communications," *IEEE Trans. Antennas Propag.*, vol. 52, no. 11, pp. 2810–2824, Nov. 2004, doi: 10.1109/TAP.2004.835272.

[2] R. Janaswamy, "Effect of element mutual coupling on the capacity of fixed length linear arrays," *IEEE Antennas Wirel. Propag. Lett.*, vol. 1, pp. 157–160, 2002, doi: 10.1109/LAWP.2002.807570.

[3] Z. Qamar, U. Naeem, S. A. Khan, M. Chongcheawchamnan, and M. F. Shafique, "Mutual Coupling Reduction for High-Performance Densely Packed Patch Antenna Arrays on Finite Substrate," *IEEE Trans. Antennas Propag.*, vol. 64, no. 5, pp. 1653–1660, May 2016, doi: 10.1109/TAP.2016.2535540.

[4] M. S. Khan, M. F. Shafique, A. Naqvi, A. D. Capobianco, B. Ijaz, and B. D. Braaten, "A miniaturized dual-band MIMO antenna for WLAN applications," *IEEE Antennas Wirel. Propag. Lett.*, vol. 14, pp. 958–961, Dec. 2015, doi: 10.1109/LAWP.2014.2387701.

[5] J. H. Xun, L. F. Shi, W. R. Liu, G. X. Liu, and S. Chen, "Compact Dual-Band Decoupling Structure for Improving Mutual Coupling of Closely Placed PIFAs," *IEEE Antennas Wirel. Propag. Lett.*, vol. 16, pp. 1985–1989, 2017, doi: 10.1109/LAWP.2017.2691716.

[6] B. L. Dhevi, K. S. Vishvaksenan, and K. Rajakani, "Isolation Enhancement in Dual-Band Microstrip Antenna Array Using Asymmetric Loop Resonator," *IEEE Antennas Wirel. Propag. Lett.*, vol. 17, no. 2, pp. 238–241, Feb. 2018, doi: 10.1109/LAWP.2017.2781907.

[7] S. Nandi and A. Mohan, "A compact dual-band MIMO slot antenna for WLAN applications," *IEEE Antennas Wirel. Propag. Lett.*, vol. 16, pp. 2457–2460, Jul. 2017, doi: 10.1109/LAWP.2017.2723927.

[8] J. Sui and K. L. Wu, "A General T-Stub Circuit for Decoupling of Two Dual-Band Antennas," *IEEE Trans. Microw. Theory Tech.*, vol. 65, no. 6, pp. 2111–2121, Jun. 2017, doi: 10.1109/TMTT.2017.2647951.

[9] X. Ling and R. Li, "A novel dual-band MIMO antenna array with low mutual coupling for portable wireless devices," *IEEE Antennas Wirel. Propag. Lett.*, vol. 10, pp. 1039–1042, 2011, doi: 10.1109/LAWP.2011.2169035.

[10] M. S. Sharawi, A. B. Numan, M. U. Khan, and D. N. Aloi, "A dual-element dual-band MIMO antenna system with enhanced isolation for mobile terminals," *IEEE Antennas Wirel. Propag. Lett.*, vol. 11, pp. 1006–1009, 2012, doi: 10.1109/LAWP.2012.2214433.

[11] A. Boukarkar, X. Q. Lin, Y. Jiang, L. Y. Nie, P. Mei, and Y. Q. Yu, "A miniaturized extremely close-spaced four-element dual-band MIMO antenna system with polarization and pattern diversity," *IEEE Antennas Wirel. Propag. Lett.*, vol. 17, no. 1, pp. 134–137, Jan. 2018, doi: 10.1109/LAWP.2017.2777839.

[12] Y. Ding, Z. Du, K. Gong, and Z. Feng, "A novel dual-band printed diversity antenna for mobile terminals," *IEEE Trans. Antennas Propag.*, vol. 55, no. 7, pp. 2088–2096, Jul. 2007, doi: 10.1109/TAP.2007.900249.

[13] F. Liu, A. Chen, and L. Zhao, "Dual-band Antenna Decoupling Design with Stepped Impedance Loaded Dual-band Dummy Element," *2018 IEEE Antennas Propag. Soc. Int. Symp. Usn. Natl. Radio Sci. Meet. APSURSI 2018 - Proc.*, pp. 359–360, 2018, doi: 10.1109/APUSNCURSINRSM.2018.8608676.

[14] M. M. Albannay, J. C. Coetzee, X. Tang, and K. Mouthaan, "Dual-frequency decoupling for two distinct antennas," *IEEE Antennas Wirel. Propag. Lett.*, vol. 11, pp. 1315–1318, 2012, doi: 10.1109/LAWP.2012.2226635.

[15] B. C. Pan and T. J. Cui, "Broadband Decoupling Network for Dual-Band Microstrip Patch Antennas," *IEEE Trans. Antennas Propag.*, vol. 65, no. 10, p. IEEE Trans. Antennas Propag., 2017, doi: 10.1109/TAP.2017.2742539.

[16] L. Zhao and K. L. Wu, "A Dual-Band Coupled Resonator Decoupling Network for Two Coupled Antennas," *IEEE Trans. Antennas Propag.*, vol. 63, no. 7, pp. 2843–2850, Jul. 2015, doi: 10.1109/TAP.2015.2421973.

[17] I. Dioum, A. Diallo, S. M. Farssi, and C. Luxey, "A novel compact dual-band LTE antenna-system for MIMO operation," *IEEE Trans. Antennas Propag.*, vol. 62, no. 4, pp. 2291–2296, 2014, doi: 10.1109/TAP.2014.2301151.

[18] Y. F. Cheng and K. K. M. Cheng, "Novel wideband decoupling technique for MIMO antenna arrays with two independently controlled transmission zeros," *IEEE MTT-S Int. Microw. Symp. Dig.*, pp. 853–856, Oct. 2017, doi: 10.1109/MWSYM.2017.8058714.

[19] Y. F. Cheng and K. K. M. Cheng, "A Novel Dual-Band Decoupling and Matching Technique for Asymmetric Antenna Arrays," *IEEE Trans. Microw. Theory Tech.*, vol. 66, no. 5, pp. 2080–2089, May 2018, doi: 10.1109/TMTT.2018.2797101.

[20] P. L. Chi, C. J. Lee, and T. Itoh, "A compact dual-band metamaterial-based rat-race coupler for a MIMO system application," *IEEE MTT-S Int. Microw. Symp. Dig.*, pp. 667–670, 2008, doi: 10.1109/MWSYM.2008.4632920.

[21] P. L. Chi and T. Itoh, "Miniaturized Dual-band directional couplers using composite right/left-handed transmission structures and their applications in beam pattern diversity systems," *IEEE Trans. Microw. Theory Tech.*, vol. 57, no. 5, pp. 1207–1215, May 2009, doi: 10.1109/TMTT.2009.2017350.

[22] K. C. Lin, C. H. Wu, C. H. Lai, and T. G. Ma, "Novel dual-band decoupling network for two-element closely spaced array using synthesized microstrip lines," *IEEE Trans. Antennas Propag.*, vol. 60, no. 11, pp. 5118–5128, Nov. 2012, doi: 10.1109/TAP.2012.2207687.

[23] Y. Wu, Y. Liu, Y. Zhang, J. Gao, and H. Zhou, "A dual band unequal wilkinson power divider without reactive components," *IEEE Trans. Microw. Theory Tech.*, vol. 57, no. 1, pp. 216–222, 2009, doi: 10.1109/TMTT.2008.2008981.

[24] X. Tan, W. Wang, Y. Wu, Y. Liu, and A. A. Kishk, "Enhancing Isolation in Dual-Band Meander-Line Multiple Antenna by Employing Split EBG Structure," *IEEE Trans. Antennas Propag.*, vol. 67, no. 4, pp. 2769–2774, Apr. 2019, doi: 10.1109/TAP.2019.2897489.

[25] C. Guo, H. Zhai, and S. Liu, "A new dual-band microstrip antenna array with high isolation by waveguided metamaterial structure," *Microw. Opt. Technol. Lett.*, vol. 61, no. 5, pp. 1365–1370, May 2019, doi: 10.1002/mop.31707.

[26] Deepak Batra, Sanjay Sharma, Amit Kumar Kohli, "Dual-Band Dielectric Resonator Antenna for C and X Band Application," *Int. J. Antennas Propag.*, 2012, doi: https://doi.org/10.1155/2012/914201.

[27] Y. Zhang, J. Y. Deng, M. J. Li, D. Sun, and L. X. Guo, "A MIMO Dielectric Resonator Antenna With Improved Isolation for 5G mm-Wave Applications," *IEEE Antennas Wirel. Propag. Lett.*, vol. 18, no. 4, pp. 747–751, Apr. 2019, doi: 10.1109/LAWP.2019.2901961.

[28] A. Abdalrazik, A. S. A. El-Hameed, and A. B. Abdel-Rahman, "A Three-Port MIMO Dielectric Resonator Antenna Using Decoupled Modes," *IEEE Antennas Wirel. Propag. Lett.*, vol. 16, pp. 3104–3107, Oct. 2017, doi: 10.1109/LAWP.2017.2763426.

[29] K. Ishimiya, Z. Ying, and J. I. Takada, "A compact MIMO DRA for 802.11n

application," *2008 IEEE Int. Symp. Antennas Propag. Usn. Natl. Radio Sci. Meet. APSURSI*, 2008, doi: 10.1109/APS.2008.4619609.

[30] J. B. Yan and J. T. Bernhard, "Implementation of a frequency-agile MIMO dielectric resonator antenna," *IEEE Trans. Antennas Propag.*, vol. 61, no. 7, pp. 3434–3441, 2013, doi: 10.1109/TAP.2013.2255092.

[31] L. Zou, D. Abbott, and C. Fumeaux, "Omnidirectional cylindrical dielectric resonator antenna with dual polarization," *IEEE Antennas Wirel. Propag. Lett.*, vol. 11, pp. 515–518, 2012, doi: 10.1109/LAWP.2012.2199277.

[32] H. N. Chen, J. -M. Song and J. -D. Park, "A Compact Circularly Polarized MIMO Dielectric Resonator Antenna Over Electromagnetic Band-Gap Surface for 5G Applications," *IEEE Access*, vol. 7, pp. 140889–140898, 2019, doi: 10.1109/ACCESS.2019.2943880.

[33] A. Dadgarpour, B. Zarghooni, B. S. Virdee, T. A. Denidni, and A. A. Kishk, "Mutual Coupling Reduction in Dielectric Resonator Antennas Using Metasurface Shield for 60-GHz MIMO Systems," *IEEE Antennas Wirel. Propag. Lett.*, vol. 16, pp. 477–480, 2017, doi: 10.1109/LAWP.2016.2585127.

[34] G. Das, A. Sharma, R. K. Gangwar, and M. S. Sharawi, "Performance improvement of multiband MIMO dielectric resonator antenna system with a partially reflecting surface," *IEEE Antennas Wirel. Propag. Lett.*, vol. 18, no. 10, pp. 2105–2109, Oct. 2019, doi: 10.1109/LAWP.2019.2938004.

[35] A. Ahmad Khan, R. Khan, S. Aqeel, J. Ur Rehman Kazim, J. Saleem, and M. K. Owais, "Dual-band mimo rectangular dielectric resonator antenna with high port isolation for LTE applications," *Microw. Opt. Technol. Lett.*, vol. 59, no. 1, pp. 44–49, Jan. 2017, doi: 10.1002/mop.30217.

[36] Aftab Ahmad Khan, Mohd Haizal Jamaluddin, Sajid Aqeel, Jamal Nasir, Jalil ur Rehman Kazim, Owais Owais, "Dual-band MIMO dielectric resonator antenna for WiMAX/WLAN applications," *IET Microwaves, Antennas Propag.*, 2017, doi: https://doi.org/10.1049/iet-map.2015.0745.

[37] W. Sun, Y. Li, L. Chang, H. Li, X. Qin, and H. Wang, "Dual-band dual-polarized microstrip antenna array using double-layer gridded patches for 5g millimeter-wave applications," *IEEE Trans. Antennas Propag.*, vol. 69, no. 10, pp. 6489–6499, Oct. 2021, doi: 10.1109/TAP.2021.3070185.

[38] S. Varghese, P. Abdulla, A. M. Baby, and P. M. Jasmine, "High-Gain Dual-Band Waveguide-Fed Dielectric Resonator Antenna," *IEEE Antennas Wirel. Propag. Lett.*, vol. 21, no. 2, pp. 232–236, Feb. 2022, doi: 10.1109/LAWP.2021.3124225.

[39] A. Muhammad, M. U. Khan, R. S. Malfajani, M. S. Sharawi and M. Alathbah, "An Integrated DRA-Based Large Frequency Ratio Antenna System Consisting of a MM-Wave Array and a MIMO Antenna for 5G Applications," *IEEE Open J. Antennas Propag.*, vol. 5, no. 2, pp. 368–378, 2024, doi: 10.1109/OJAP.2024.3349455.

[40] L. Huitema and T. Monediere, "Dielectric Materials for Compact Dielectric Resonator Antenna Applications," *Dielectr. Mater.*, vol. 10, 2012, [Online]. Available: https://www.intechopen.com/chapters/39573